ORIGINAL ARTICLE

lajss.org Latin American Journal of Solids and Structures

www.lajss.org

Mechanical and Energy-Absorption Properties of a 3D-Printed Star-Shaped Auxetic Honeycomb under Combined Compression-Shear Loading

Geng Luo[a], Duanyu Mo[a], Chengpeng Chai[a], Junzhe Liu[a], Yisong Chen[a]*

[a] School of Automobile, Chang'an University, Xi'an, 710064, China. Email: luogeng@chd.edu.cn, moduanyu@163.com, chaicp@chd.edu.cn, liujunzhe1998@chd.edu.cn, chenyisong_1988@chd.edu.cn

* Corresponding author

https://doi.org/10.1590/1679-78257624

Abstract

In this study, we investigated the mechanical and energy-absorption properties of a star-shaped auxetic honeycomb under combined compression-shear loading. Novel fixtures were designed to conduct quasi-static combined compression-shear loadings. Experimental and numerical results show that the honeycomb undergoes an overall deformation based on cell rotation under quasi-static loading, producing an inclined deformation band. The normal yield stress decreased, and the shear yield stress increased with an increase in the loading angle. The extrusion deformation between meso-structures became more sufficient under dynamic combined loadings. The material deformation mode changed from overall deformation to local deformation accompanied by the formation of a shock wave. The yield criteria were established based on the ellipse equation. With an increase in the loading angle, the energy absorption in the normal and shear directions of the materials showed downward and upward trends, respectively. A theoretical model was proposed based on the 1D shock wave model to predict the energy-absorption behaviour under dynamic loading.

Keywords

Auxetic honeycomb; Combined loading; Yield surface; Energy absorption

Graphical Abstract

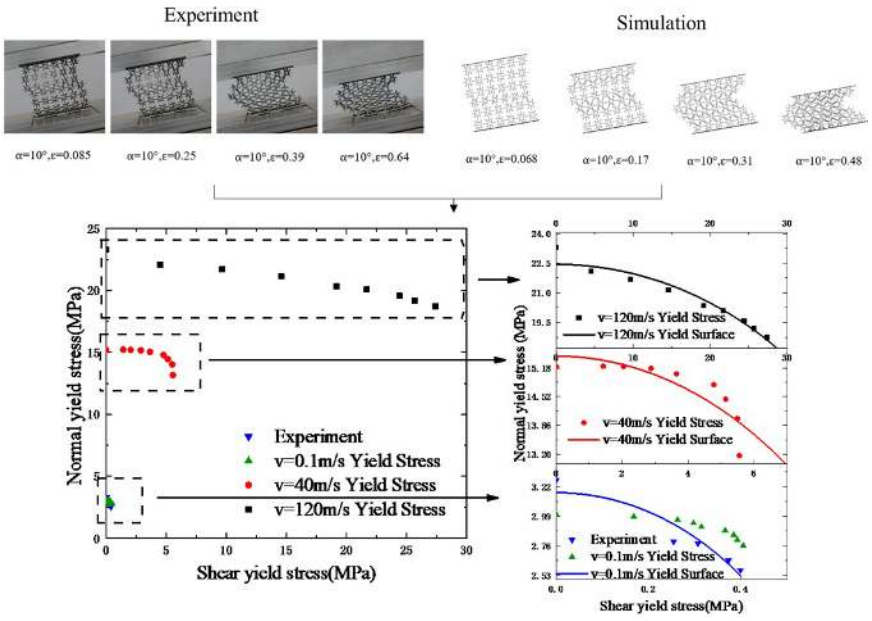

Received: April 07, 2023. In revised form: April 10, 2023. Accepted: April 17, 2023. Available online: April 20, 2023.
https://doi.org/10.1590/1679-78257624

Latin American Journal of Solids and Structures. ISSN 1679-7825. Copyright © 2023. This is an Open Access article distributed under the terms of the Creative Commons Attribution License, which permits unrestricted use, distribution, and reproduction in any medium, provided the original work is properly cited.

1 INTRODUCTION

Auxetic honeycombs have a negative Poisson's ratio and exhibit unique mechanical properties of transverse shrinkage under pressure. Compared with traditional materials, they have better performance in terms of impact resistance, energy absorption, etc., and have been widely used in various engineering applications (S. D. Rapaka et al, 2020). They are typically subjected to combined compression-shear loading, particularly dynamic loadings, under which the behaviour differs from that under uniaxial quasi-static loading. Therefore, it is important to study the mechanical and energy-absorption properties under combined compression-shear loading.

Auxetic materials have attracted the attentions in recent years. Gibson and Ashby (1982) and Gibson et al. (1982) prepared rubber and aluminium honeycombs with auxetic properties firstly. Lakes (1987) prepared foams with auxetic properties, and several new auxetic material microstructures and design methods have been rapidly developed. Materials with auxetic properties, including star-shaped honeycombs, double-arrow structures, concave structures, and chiral structures, have been proposed and studied widely (M. Xu et al, 2020; T. Wang et al, 2022; C. Qi et al, 2022). Dong et al. (2019) conducted an in-plane compression experiment and simulation of a concave hexagonal honeycomb, and clarified the influence of cell wall thickness on the material deformation mode. Wang et al. (2019) proposed a double-arrow honeycomb based on a traditional star-shaped material and explored the in-plane crushing behaviour of a material under static and impact loads using the finite element method. The results show that the double-arrow honeycomb has a better energy-absorption effect under low-speed impact. Wei et al. (2020; 2021) proposed a star-shaped triangular honeycomb expansion material by replacing the horizontal ligament of the star-shaped honeycomb with a triangular structure. It was pointed out that the energy absorption of the triangular honeycomb in the vertical direction was significantly higher than that in the horizontal direction. Currently, most studies on auxetic materials are limited to uniaxial compression. The auxetic materials are mostly subjected to combined compression-shear loads in the engineering applications. The mechanical and energy absorption properties of auxetic honeycombs under combined compression-shear loads have not been studied thoroughly in literature.

The mechanical properties of traditional honeycombs under complex stress states have been reported in literature. For example, Ashab et al. (2016) used specially designed clamps to investigate out-of-plane complex loading on an aluminium honeycomb with different cell sizes and wall thicknesses at loading angles of 15°, 30°, and 45°. The relationship between the platform stress, energy-absorption characteristics, loading plane, and loading angle of the materials was discussed in detail. Hou et al. (2011a, b) conducted dynamic experiments and simulations based on Hopkinson bars, and explored the mechanical behaviour of an aluminium honeycomb under multiaxial impact loads. The results showed that the normal peak load and platform stress of the materials decreased with an increase in the loading angle, and the material stress curve was significantly enhanced under an impact load. Ashab et al. (2014) investigated the deformation mechanism of different types of aluminum honeycombs under quasi-static out of plane combined loading, and obtained the effects of cell size and cell wall thickness. Hong et al. (2008) conducted an inclined load experiment on an aluminium honeycomb under compression-dominated conditions to obtain the yield surface at different loading speeds, and described a macroscopic yield criterion as a function of the impact velocity. However, studies on complex loading conditions of traditional honeycombs are limited to the out-of-plane direction. In fact, for auxetic honeycomb, the negative Poisson's ratio effect is only exhibited in the in-plane direction. The current research (A. Ingrole et al, 2017; F. Xu et al, 2021; C. Qi et al, 2019; J. Qiao, and C. Q. Chen, 2015) mostly focused on the design of meso-structure and the mechanical properties of auxetic honeycombs under in-plane uniaxial compression. The mechanical behavior and energy absorption properties of honeycomb under the combined compression-shear loading condition are still less investigated. In engineering applications, the characteristics of the in-plane direction are primarily leveraged for energy absorption. Therefore, the above investigations on the mechanical properties combined of traditional honeycomb under out of plane combined loading may not be of guiding significance for the mechanical properties of auxetic materials.

In recent years, the rapid development of 3D printing technology has made it possible to prepare various types of cellular materials with complex meso-structures (R. Gümrük, and R. A. W. Mines, 2013; R. A. W. Mines et al, 2013; C. Yang, and S. Kyriakides, 2019). In this study, a star-shaped auxetic honeycomb was produced using additive manufacturing technology, and a quasi-static combined compression-shear loading test was conducted. Combined with finite element analysis, the energy-absorption characteristics and mechanical behaviour of the materials under various loading conditions were studied. The theoretical model was established based on ellipse equation. The investigations can serve as benchmarks for exploring the in-plane mechanical behaviour and energy-absorption characteristics of auxetic honeycomb.

2 FIGURES QUASI-STATIC COMBINED COMPRESSION-SHEAR EXPERIMENT

2.1 Specimen

A star-shaped auxetic honeycomb is an auxetic material based on a concave hexagonal honeycomb that introduces a concave structure in the vertical direction (Figure 1). In Figure 1, l is the length of the inclined cell wall, h is the horizontal and vertical rib length, t is the thickness of the cell wall, and θ is the angle between the inclined cell wall and vertical direction.

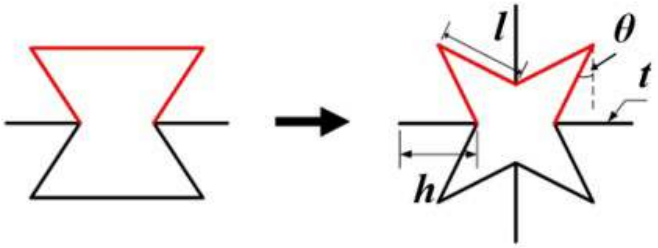

Figure 1. Star-shaped auxetic honeycomb and its geometric parameters.

An ISLM280 3D printer from Zhongrui Technology was selected, and a laser selective melting process was adopted. The spot diameter was 0.1 mm, and scanning speed was 6 m/s. The laser power was 200W, and the printing substrate was 316L stainless steel. The specific material parameters of the 316L base material were obtained through a tensile experiment (Figure 2), as shown in Table 1. The strain rate of the matrix material 316L is insensitive (Obadimu and Kourousis, 2023). To avoid the size effect (L. Li et al, 2016) on the experimental results, the star-shaped honeycomb specimen adopted a layout of 6 × 6 cells (Figure 3), and the meso-structural parameters are shown in Table 2. The relative density of a regular honeycomb significantly affects the energy-absorption capacity of the material and deformation mode (X. Niu et al, 2022). The relative density of the honeycomb can be expressed as the ratio of the area of the solid part of the cell to the area of its corresponding rectangular cross section, given by (Z. Dong et al., 2019)

$$\bar{\rho}_{SH} = \frac{\rho_{SH}^*}{\rho_s} = \frac{t}{h}\frac{\left(1+\frac{2l}{h}\right)}{\left[1+\sqrt{2}l\sin\left(\frac{\pi}{4}\right)-\theta\right]^2} \tag{1}$$

where ρ_{SH}^* is the apparent density of the star-shaped auxetic honeycomb (kg/m3) and ρ_s is the density of the base material (kg/m^3).

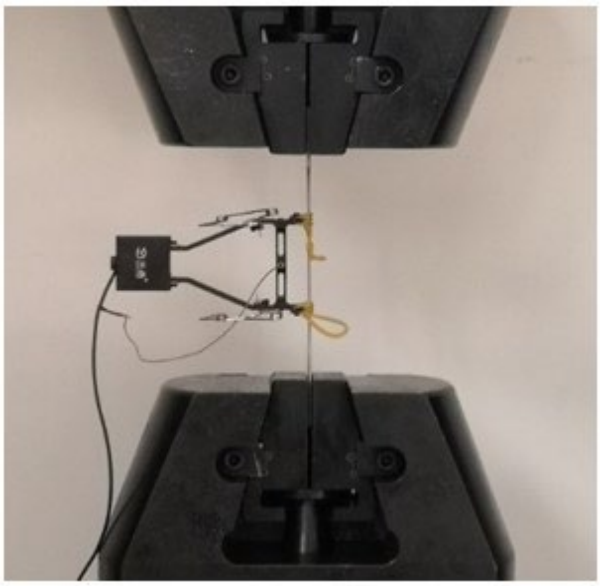

Figure 2. Tensile experiment of 316L stainless steel substrate.

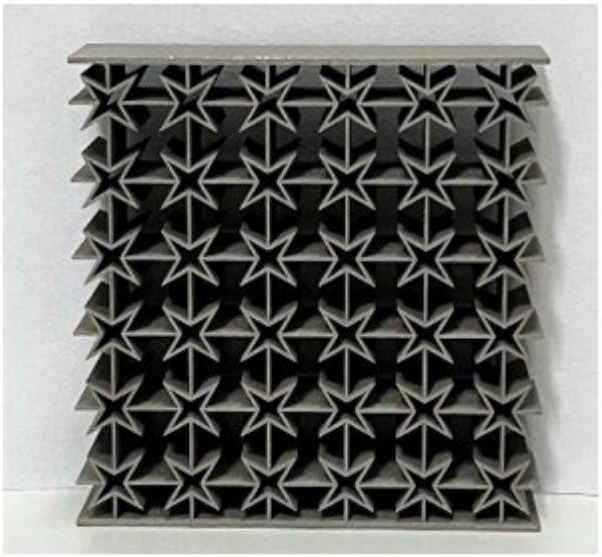

Figure 3. Star-shaped auxetic honeycomb specimen.

Table 1. Material parameters of the 316L stainless steel.

E_s	ρ_s	υ	σ_s
193 GPa	8000 kg/m^3	0.27	486 MPa

Table 2. Meso-structural parameters of star-shaped auxetic honeycomb

l	h	t	θ
4 mm	4 mm	0.5 mm	30°

2.2 Experimental setup

The combined compression-shear loading system was designed based on the Doyoyo's experiment (Doyoyo and Mohr, 2003), as shown in Figure 4. The universal machine used in the experiment was SANS CMT-5205. The loading system comprised a variable-angle complex loading fixture, an FC3D160 series three-way force sensor, and a data acquisition system. The variable-angle loading fixture was improved by installing a three-way force sensor on the lower disc based on the fixture, which comprising the upper fixed claw, upper loading disc, lower fixed claw, and lower loading disc (Figure 5). The specimen was clamped through a middle groove, and different loading angles were achieved by adjusting the angle of the loading fixture. A digital camera was used to record the deformation process of the specimen.



Figure 4. Combined compression–shear loading system.

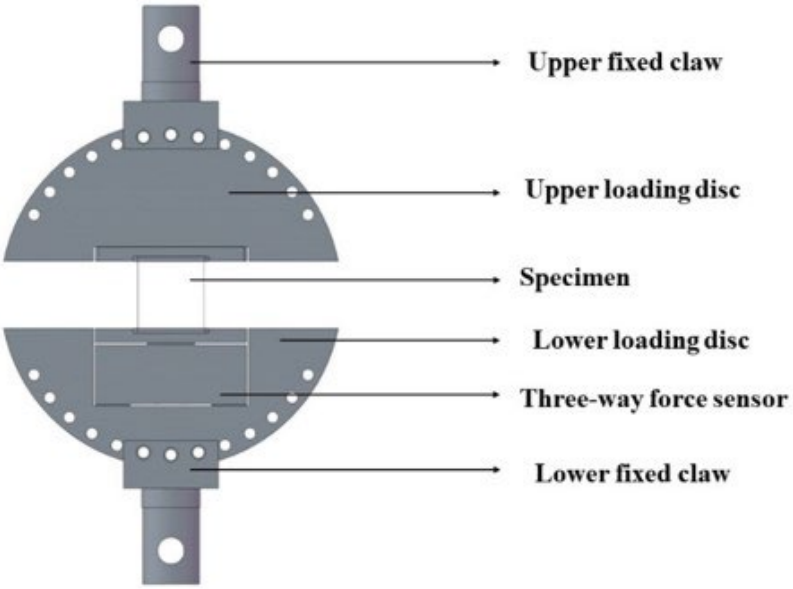

Figure 5. Variable-angle loading fixture.

2.3 Experimental results

Figures 6 and 7 show the normal and shear loading-displacement curves of the star-shaped auxetic honeycomb under combined loading, respectively. The α is the angle between the loading direction and the normal direction of the honeycomb material. As shown in Figure 6, the normal load-displacement curve of the material presents three typical stages: the elastic stage (the load increases continuously), platform stage (the load fluctuates around a constant value), and densification stage (the load value rises rapidly). The yield load exhibited a downward trend with an increase in the loading angle. The shear load-displacement curve (Figure 7) shows significant fluctuations, and the densification displacement is significantly improved with an increase in the loading angle. Figure 8 shows the deformation behaviour of the star-shaped materials under complex loading conditions. The ε is the normal nominal strain of the honeycomb material. With the increase of loading angle, the deformation mode of materials changes from “>” type to “S” type. The analysis of the material deformation mode and mechanical properties will be discussed in detail in subsequent sections.

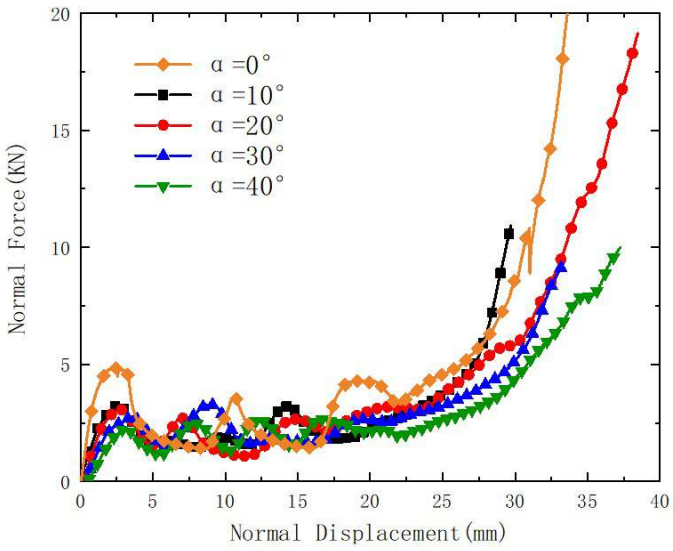

Figure 6. Normal load-displacement curve of star-shaped auxetic honeycomb under complex loading.

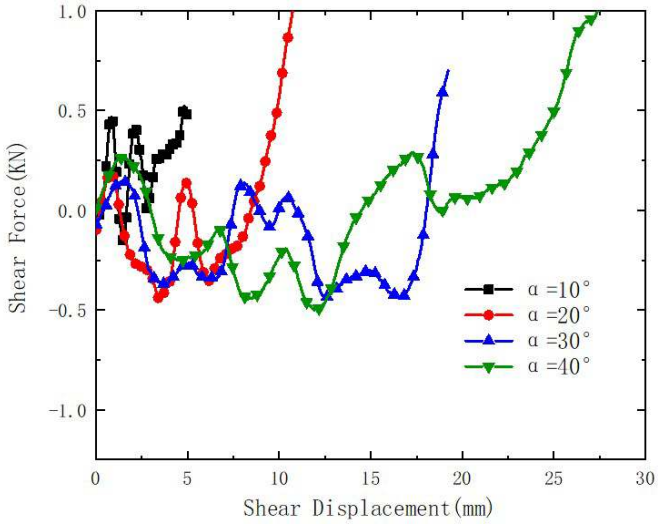

Figure 7. Shear load-displacement curve of star-shaped auxetic honeycomb under complex loading.

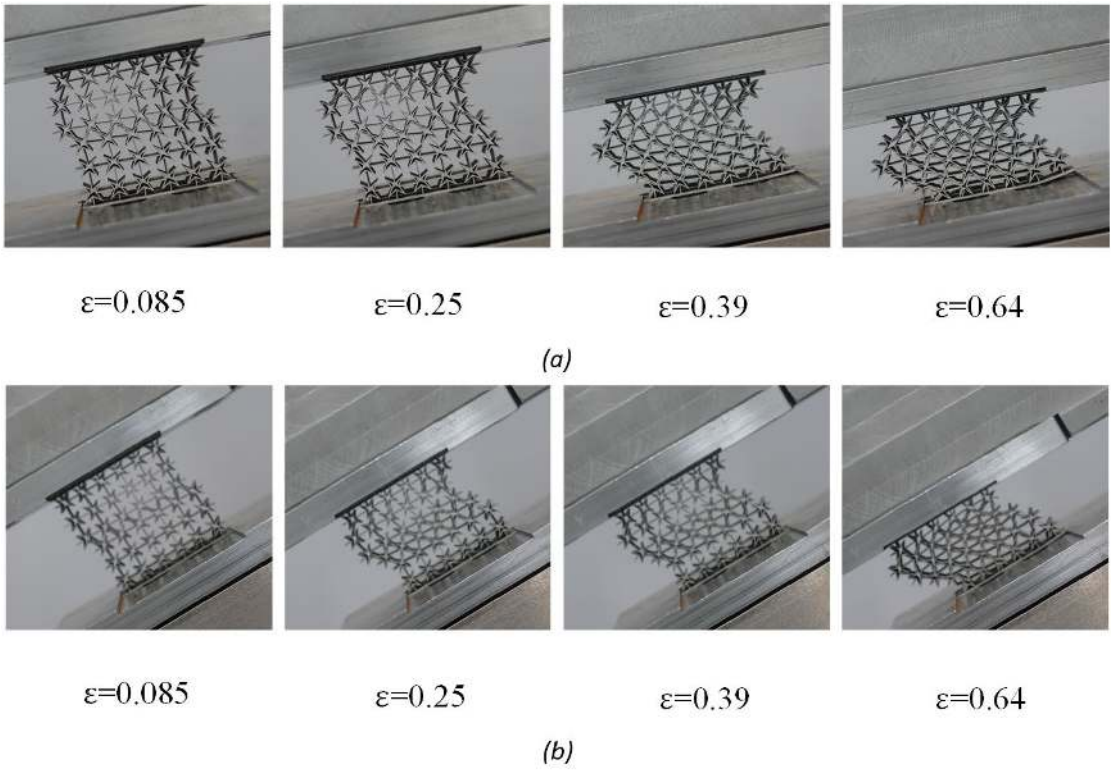

Figure 8. Deformation mode of star-shaped auxetic honeycomb specimen under complex loading: (a) α=10°; (b) α=30°

3 SIMULATION

3.1 Finite element model

Combined compression-shear simulations of the star-shaped auxetic honeycomb were conducted using ABAQUS/Explicit. The numerical model is shown in Figure 9, where α is the angle between the normal and the y-axis of the upper loading plate The upper loading plate and lower fixing plate are rigid bodies described by R3D4 discrete rigid body elements. The honeycomb element was an S4R shell element, and the base material was 316L stainless steel. The stress-strain curve of the material model is shown in Figure 10. Five integration points were defined along the thickness direction of the element. All degrees of freedom of the upper plate, except the loading direction, were constrained, and a constant speed load was applied. The lower plate constrains all degrees of freedom and binds the honeycomb.

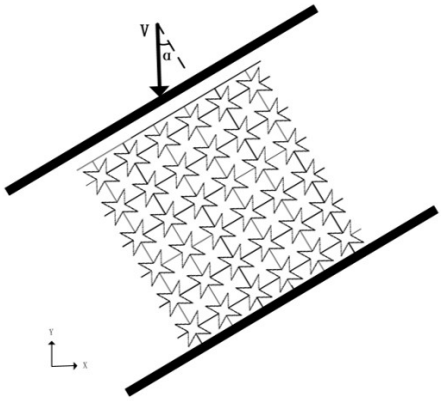

Figure 9. Complex loading simulation model.

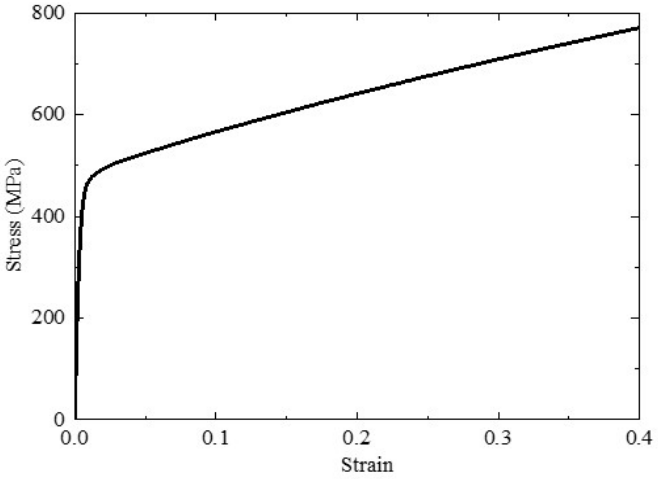

Figure 10. Stress-strain curve of 316L

3.2 Verification

Comparisons of the curves and deformation modes between simulation and experiment are shown in Figures 11-13 and Figures 14-15, respectively. It can be seen from the figures that the numerical results are consistent with the experimental results, which verifies that the finite element model established in this paper has high accuracy and can be used for subsequent research.

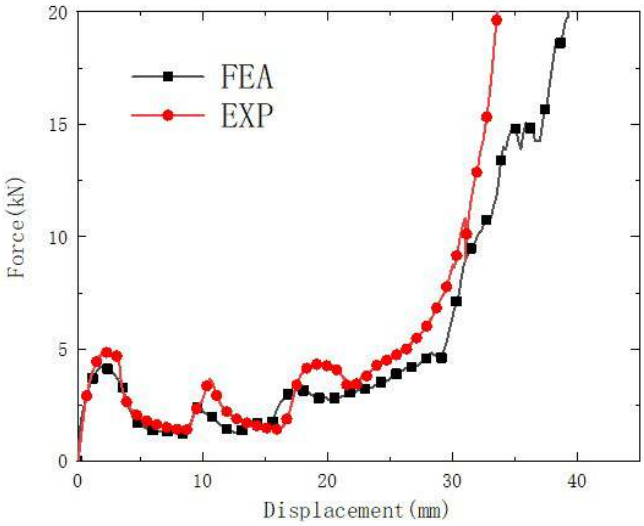

Figure 11. Comparison between numerical and experimental results of uniaxial compression load displacement(α = 0°).

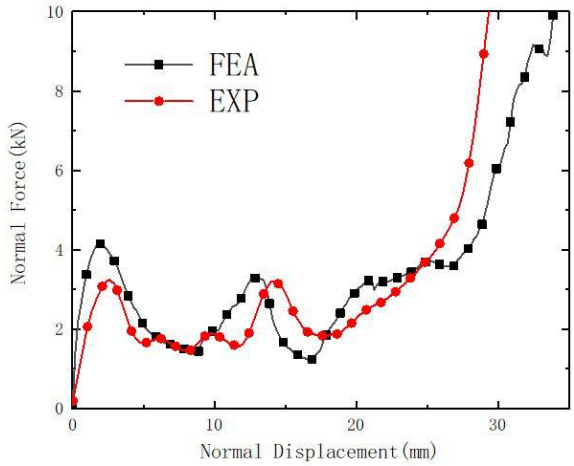

Figure 12. Comparison of normal load displacement simulation and experimental results under combined loading(α = 10°).

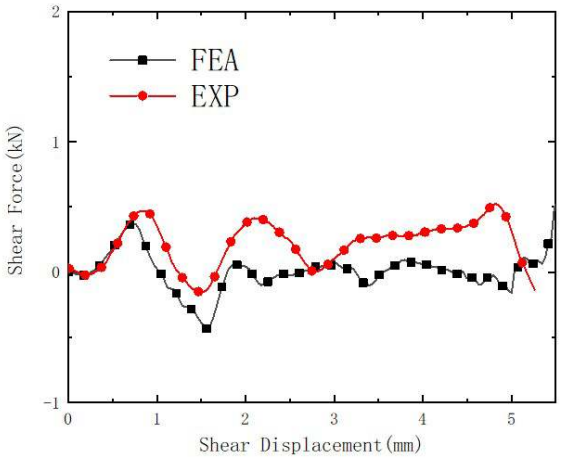

Figure 13. Comparison of shear load displacement simulation and experimental results under combined Loading(α = 10°).

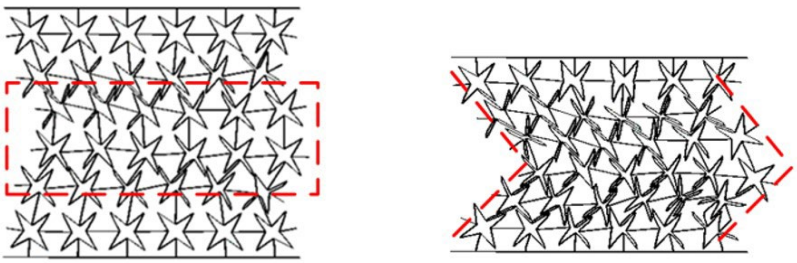

(a)

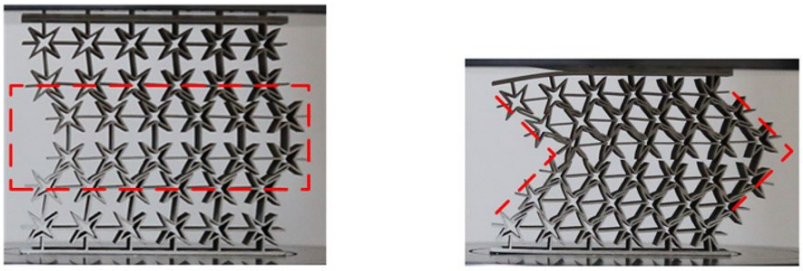

(b)

Figure 14. Comparison of complex loading experimental and simulation deformation mode results(α = 0°): (a) Simulation ; (b) Experiment

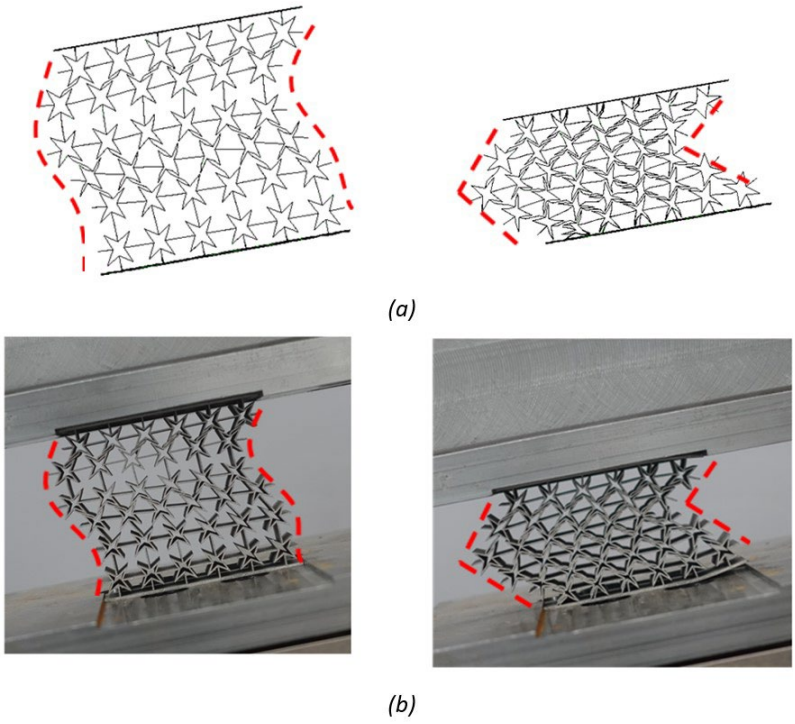

Figure 15. Comparison of complex loading experimental and simulation deformation mode results(α = 10°): (a) Simulation ; (b) Experiment

4 ANALYSIS OF RESULTS

4.1 Deformation mode

Figure 16 to Figure 18 show the deformation behaviour of a star-shaped auxetic honeycomb under different loading conditions. It is observed that with an increase in the loading speed, the deformation modes of the SAH can be divided into three modes: overall deformation, progressive deformation, and collapse deformation. When loading at low speed (v = 0.1 m/s), the material deforms uniformly. At the initial stage, the cells in the middle cell layer rotated under the effect of combined loading (Figure 16). Plastic hinges were formed at the corners of the adjacent interlaminar ribbons and cells (Figure 19). Then, the material collapsed until densification.

When the loading speed was 40 m/s, the inertia effect of the honeycomb was enhanced, and a local deformation band formed at the loading end (Figure 17). At the initial stage, the cells deformed layer-by-layer until all the cells were necked. Extrusion deformation occurred between the cell wall and rib band, and the material was crushed until densification.

When the loading speed was 120 m/s, part of the material close to the loading end completely collapsed (Figure 18), and the deformation of the material was dominated by the plastic shock wave formed by the collapse of local cells. The wavefront cell wall deformed with the rib band, extruded the adjacent cell layer, and propagated to the fixed end until the material underwent densification. Simultaneously, the inclination of the plastic shock wave band increased with an increase in the loading angle.

When honeycombs were subjected to high speeds, the cells near the impact end first deformed firstly, and then propagated to the support side forming a plastic shock wave. The cells behind the plastic wave front move together with the impact side along the normal direction to the support end. It is also noted that under combined loadings, the material cell layer showed negative Poisson's ratio characteristics at the initial stage under medium-speed loading. At low and high loading speeds, the negative Poisson's ratio characteristics of the materials were not observed.

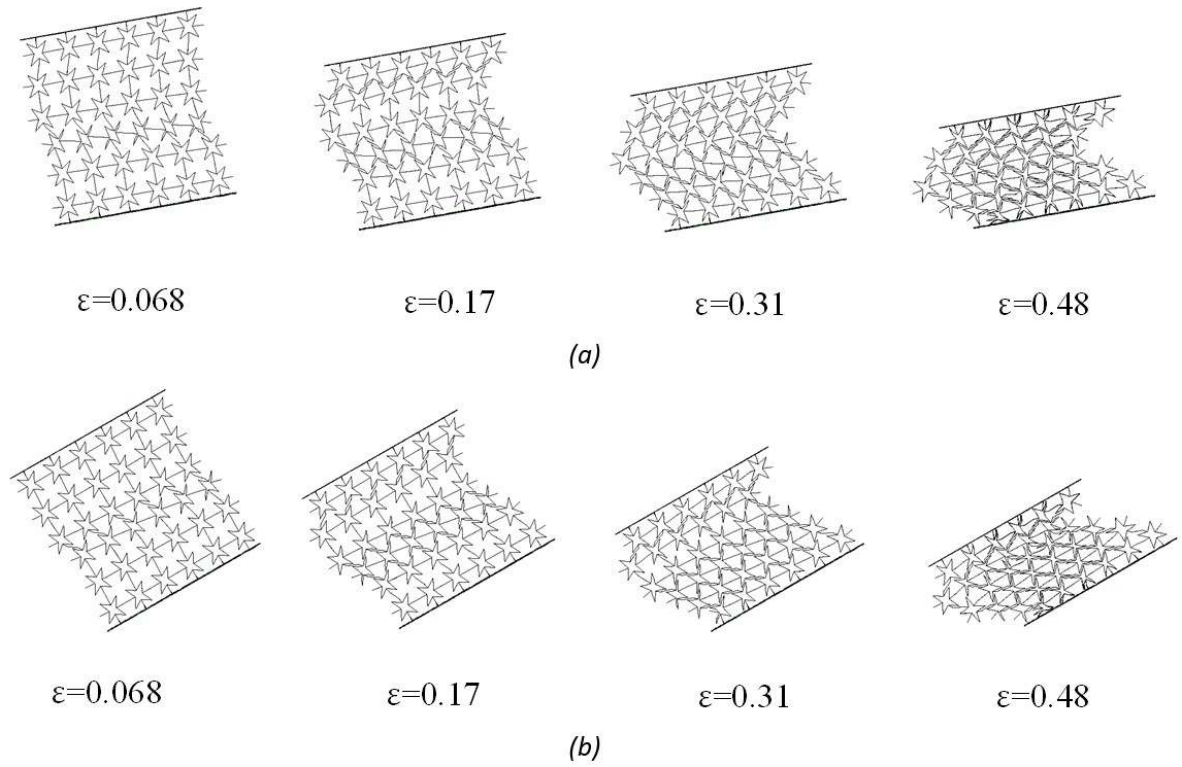

Figure 16. Deformation mode of star-shaped auxetic honeycomb under combined compression and shear loading (v = 0.1 m/s): (a) α=10°; (b) α=30°

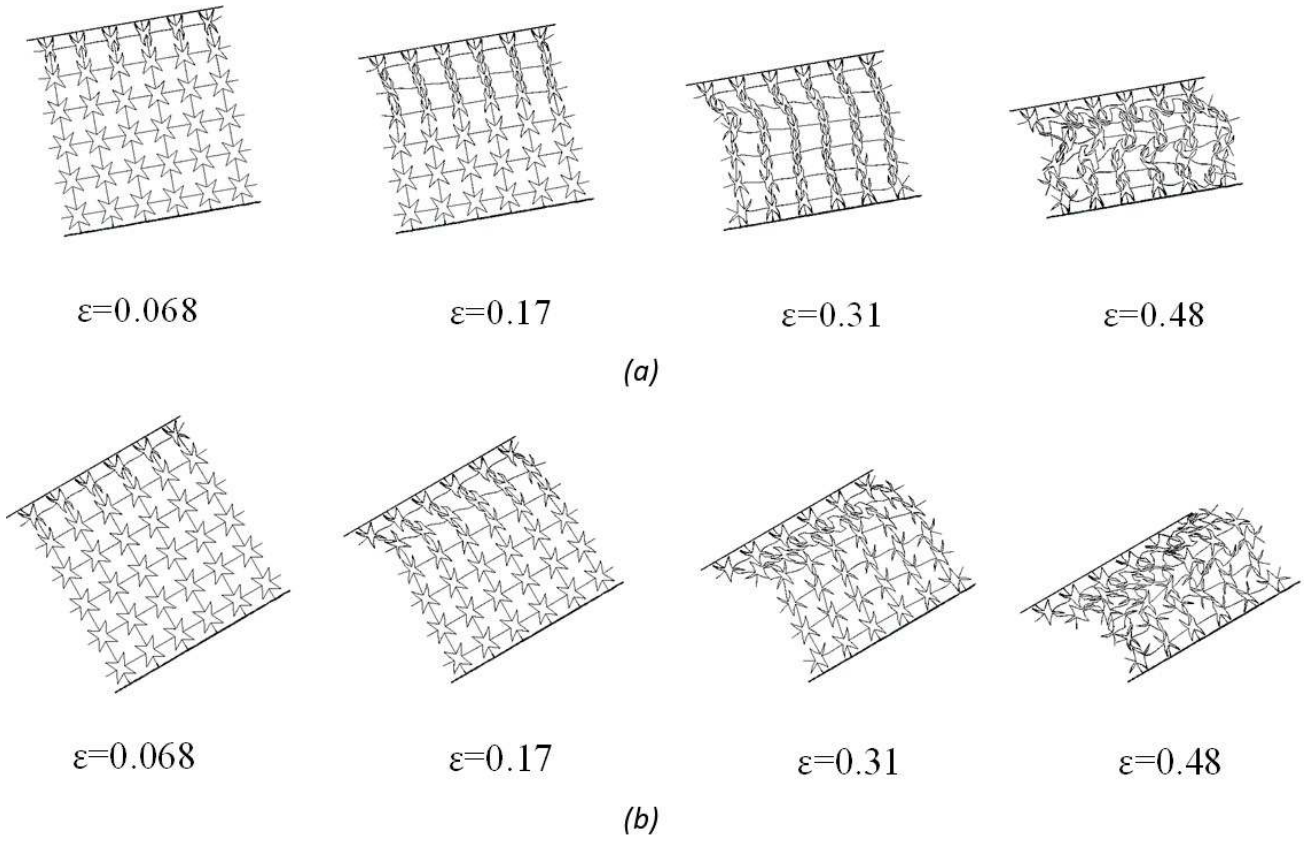

Figure 17. Deformation mode of star-shaped auxetic honeycomb under combined compression and shear loading (v = 40 m/s): (a) α=10°; (b) α=30°

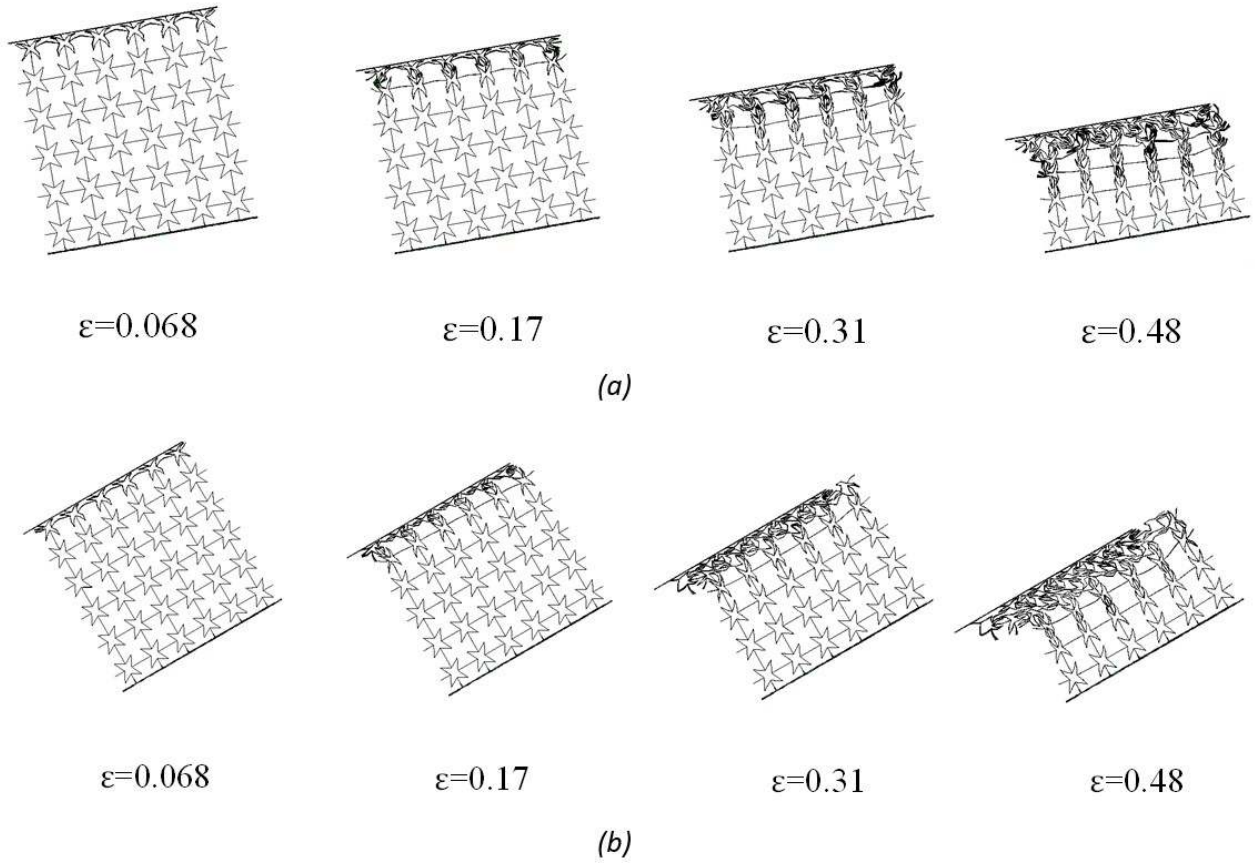

Figure 18. Deformation mode of star-shaped auxetic honeycomb under combined compression and shear loading (v = 120m/s): (a) α=10°; (b) α=30°

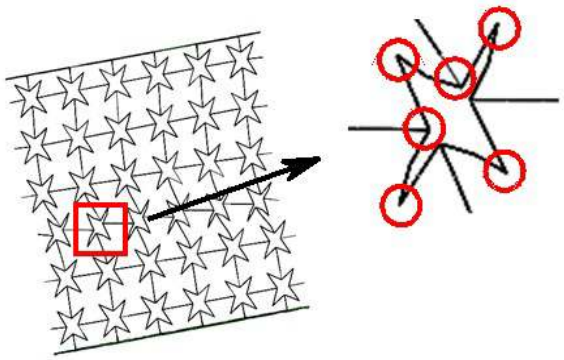

Figure 19. Deformation behaviour under low-speed loading.

4.2 Stress-strain curves

The stress-strain curves of star-shaped auxetic honeycomb under compression of 0.1 m/s, 40 m/s, and 120 m/s are shown in Figure 20 to Figure 22. The platform section of the normal stress was significantly extended with an increase in loading speed due to the enhancement of the inertia effect. With an increase in the loading angle, the densification strain only shows a slight downward trend, but the stress fluctuation behaviour of the platform section is significantly obvious. With an increase in the loading angle and shear deformation displacement, the shear densification strain of the material increased significantly. With the increase of loading speed, the honeycomb deformation mode changes from overall rotation deformation to local crushing deformation, which make the normal and shear stress plateau tended to be stable.

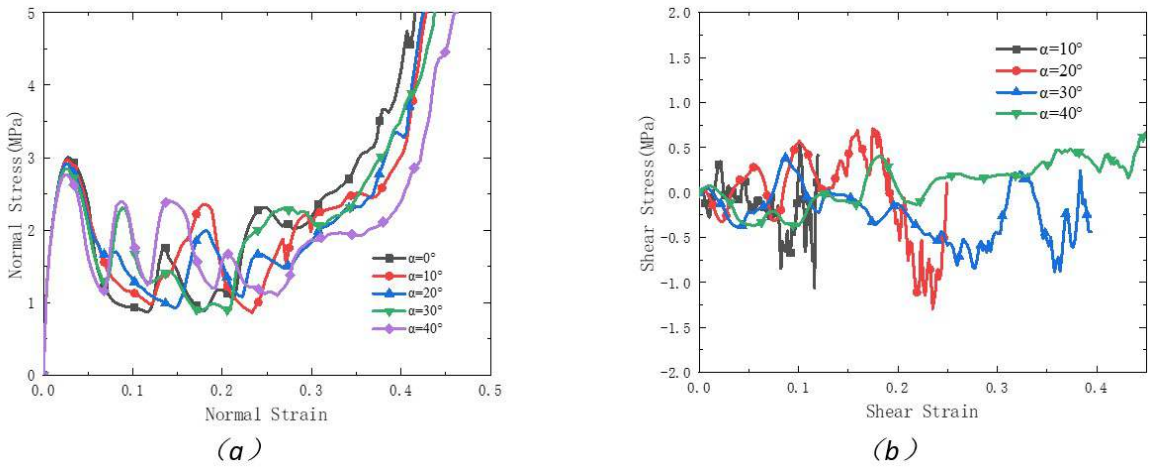

Figure 20. Stress–strain curves of star-shaped auxetic honeycomb under low-speed (v = 0.1 m/s) combined compression–shear loading: (a) Normal direction; (b) Shear direction.

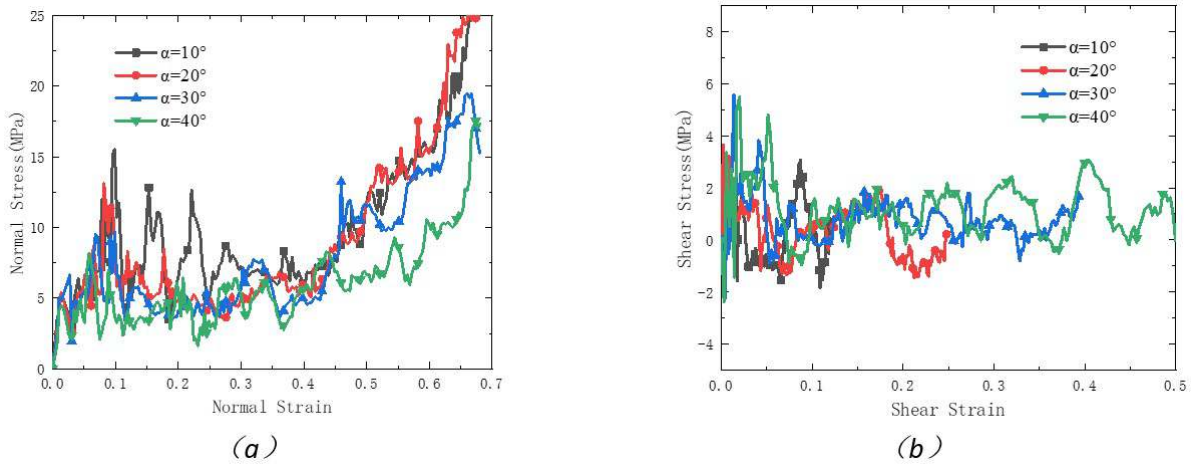

Figure 21. Stress–strain curve of star-shaped auxetic honeycomb under medium-speed (v = 40 m/s) combined compression–shear loading: (a) Normal direction; (b) Shear direction.

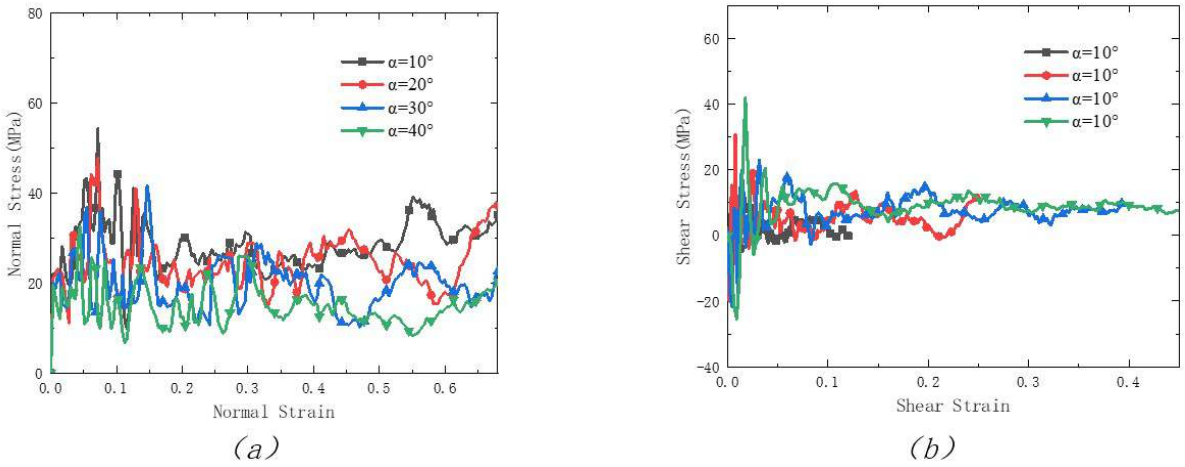

Figure 22. Stress–strain curve of star-shaped auxetic honeycomb under high-speed (v = 120 m/s) combined compression–shear loading: (a) Normal direction; (b) Shear direction.

The change of the deformation mode is mainly dependent on the loading speed, resulting in the variation in the stress-stain curves. Hence, taking α=10° as an example, the relationship between the deformation mode and the stress-stain curve at different speeds of the auxetic honeycomb were analyzed.

When the loading speed was 0.1 m/s, the material underwent overall deformation. As shown in Figure 23, at the beginning of deformation, the stress continued to increase until the yield and stress decreased. When the adjacent cell layers were in contact, the material stress curve rose and formed a second peak (Figure 23). Subsequently, the rest of the cells rotated and deformed, and the stress curve decreased. When the cell walls of the adjacent cell layers were in full contact, the deformation was dominated by extrusion between the cell walls, and the material stress was significantly improved until densification.

In the case of medium-speed loading (v = 40 m/s), the inertia effect of the material was enhanced. In the initial stage of loading, the material stress curve rose until the cell wall contacted and extruded the rib to form the first peak. As the local deformation band moved downward layer-by-layer, the stress curve formed the second and third peaks (Figure 24) until the cell was fully necked. At this time, the material deformation changed from local deformation to global deformation. The stress curve of the material tended to be flat until densification.

When the material was loaded at high speed (v = 120 m/s), the inertial effect of the material was further enhanced(Figure 25), the initial yield stress was significantly higher than that under medium-speed and low-speed working conditions, and the total deformation of the material caused the curve to reach a more extended plateau section. Moreover, the shear and normal densification strains were significantly improved.

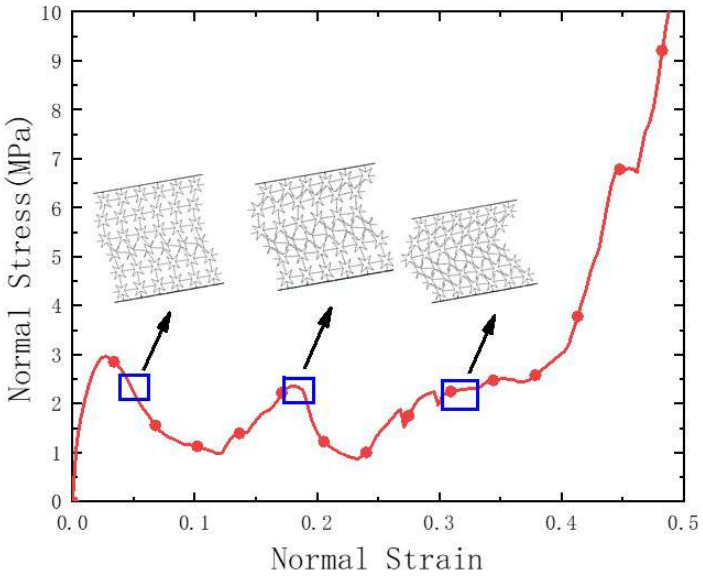

Figure 23. Stress–strain curve of star-shaped auxetic honeycomb under combined compression–shear loading(α = 10°, v = 0.1 m/s).

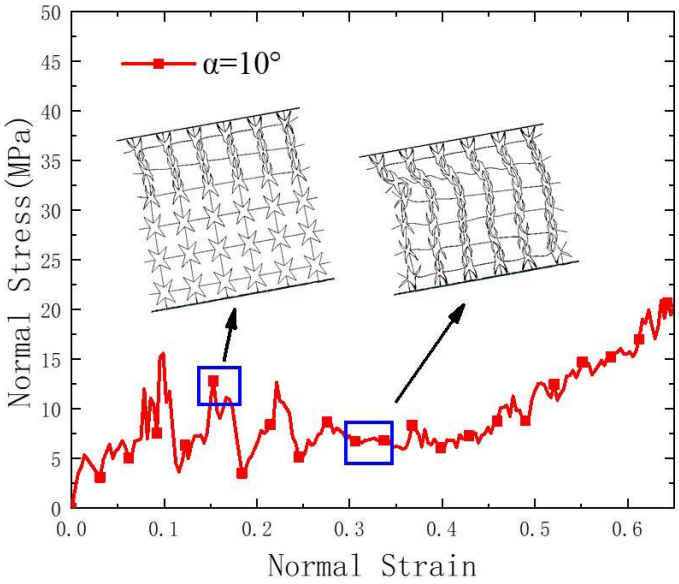

Figure 24. Stress–strain curve of star-shaped auxetic honeycomb under combined compression–shear loading(α = 10°, v = 40 m/s).

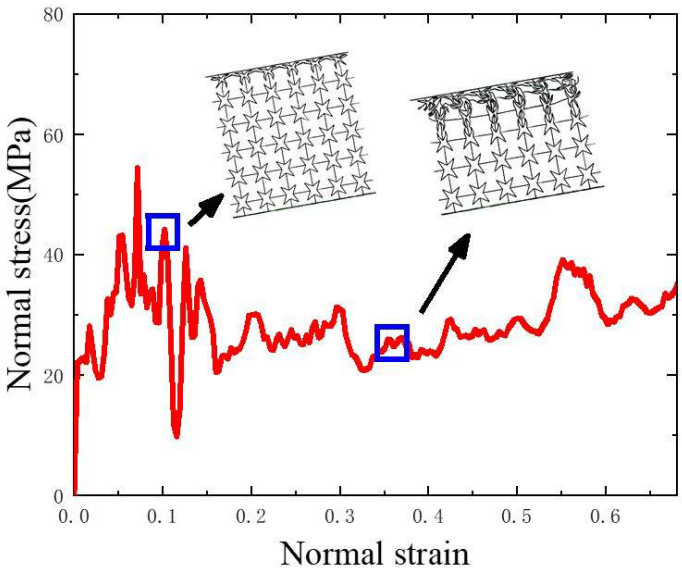

Figure 25. Stress–strain curve of star-shaped auxetic honeycomb under combined compression–shear loading(α = 10°, v = 120 m/s).

4.3 Yield surface

Figures 26 and 27 show the normal and shear yield stresses of the star-shaped auxetic honeycomb under combined compression-shear loading conditions at different loading speeds. It is observed that when the loading speed is increased, the yield stress shows a significant enhancement owing to the inertia effect. The normal and shear yield stresses of the honeycomb showed significant downward and upward trends with an increase in the loading angle, respectively.

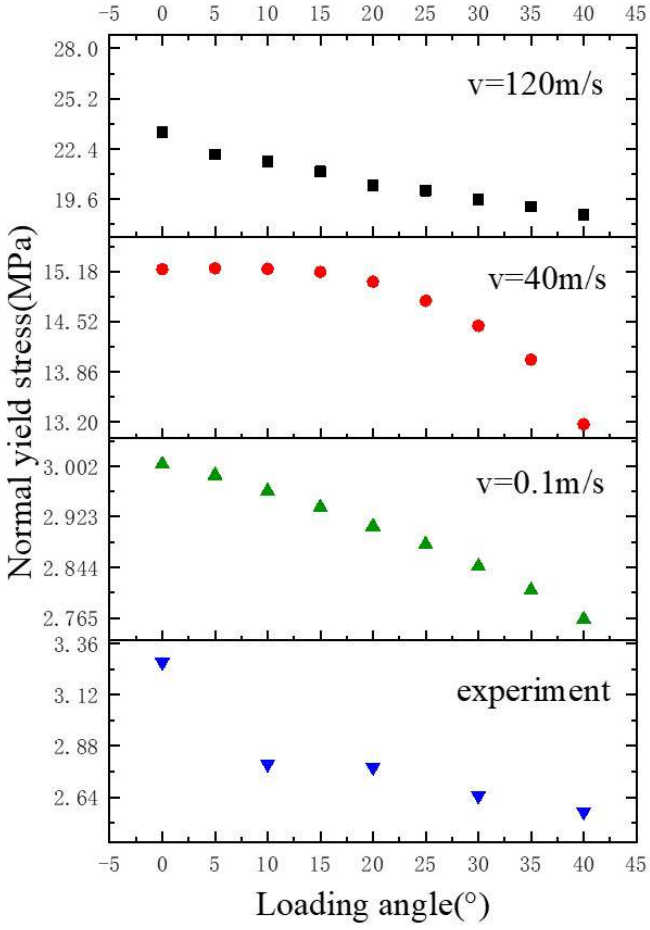

Figure 26. Normal initial yield stress.

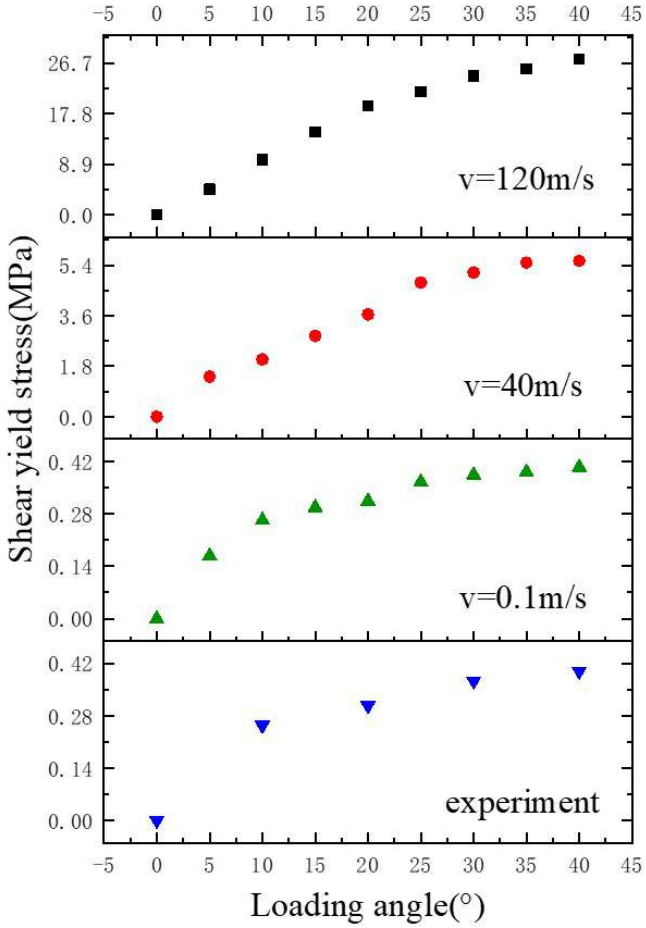

Figure 27. Shear initial yield stress.

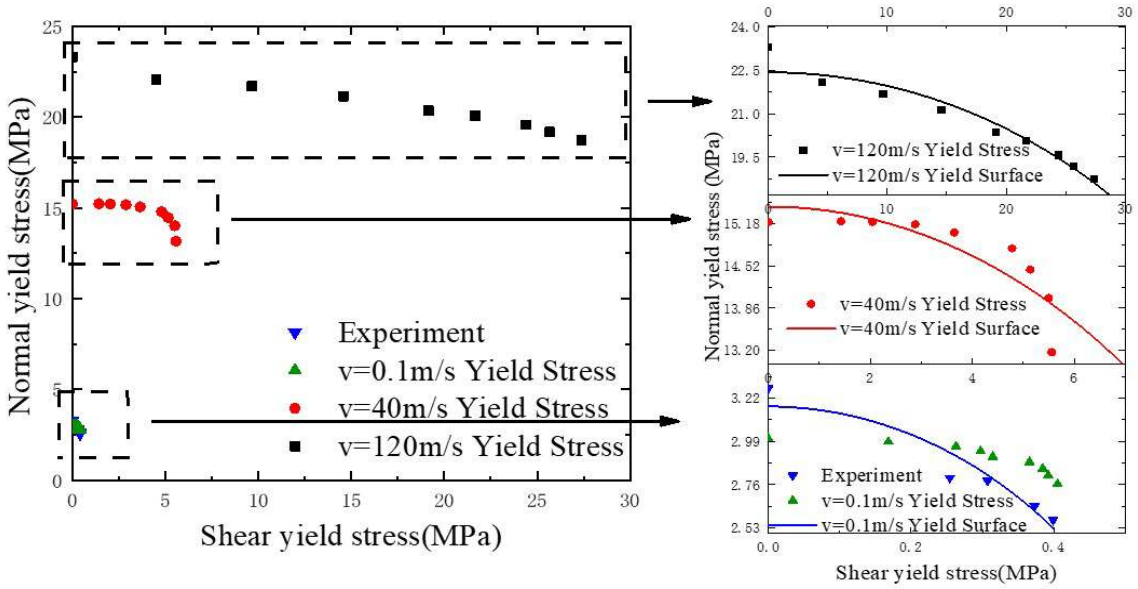

Figure 28. Yield surface of star-shaped auxetic honeycomb under combined compression–shear loadings.

The yield surface of the honeycombs under combined compression-shear loading is plotted in Figure 28. It is noted that with an increase in the loading speed, the yield surface increases, but the comparison is not isotropic. Figure 28 shows the yield surface established using the elliptic function, which is expressed as follows.

$$\left(\frac{\sigma}{\sigma_1}\right)^2 + \left(\frac{\tau}{\tau_1}\right)^2 = 1 \tag{2}$$

Here, σ_1 and τ_1 are the normal stress and shear stress of the material under dynamic loading, respectively (MPa). Under the influence of the inertia enhancement effect caused by the increase in loading speed, the normal and shear stresses of materials under dynamic conditions satisfy the following criteria (R. Gümrük, and R. A. W. Mines, 2013):

$$\sigma_1 = \sigma_0 + c_1 \frac{\rho {v_i}^2}{\varepsilon_d} \tag{3}$$

$$\tau_1 = \tau_0 + c_2 \frac{\rho {v_i}^2}{\varepsilon_d} \tag{4}$$

where σ_0 is the normal stress of the material under a static compression load (MPa); $\tau_0$is the shear stress of the material under a static shear load (MPa); c_1 and c_2 are the dynamic strengthening coefficients in the normal and shear directions, respectively; ρ is the relative density of the honeycomb; v_i is the loading speed; and ε_d is the densification strain.

The normal and shear initial yield stresses of the materials obtained from the simulation and experiment are given in Equation (2), and the Levenberg–Marquardt algorithm is used to fit the parameters. The yield surface of materials under low-speed loading (v = 0.1 m/s) can be obtained as follows:

$$\left(\frac{\sigma}{3.17}\right)^2 + \left(\frac{\tau}{0.66}\right)^2 = 1 \tag{5}$$

Under medium loading (v=40m/s), the values of σ_1 and τ_1 are 15.4 MPa and 12.8 MPa respectively. Under high loading (v=120m/s), the values of σ_1 and τ_1 are 22.4 MPa and 49.1 MPa respectively. The yield surface is shown in Equation (6).

$$\left(\frac{\sigma}{3.17+0.0037\frac{\rho {v_i}^2}{\varepsilon_d}}\right)^2 + \left(\frac{\tau}{0.66+0.0024\frac{\rho {v_i}^2}{\varepsilon_d}}\right)^2 = 1 \tag{6}$$

As shown in Figure 28, the yield stress of the material simulation and experiment is well matched when loading at a low speed (v = 0.1 m/s). With an increase in the loading speed, the dynamic initial yield surface of the material also significantly improved, showing a strengthening trend. From the compression-shear yield surface of the honeycomb, it can be observed that the loading angle has a more significant effect on the shear initial yield stress of the honeycomb. With an increase in the loading angle, the shear initial yield stress increased significantly, and the normal initial yield stress decreased to a certain extent. The influence of the loading speed on the initial yield stress of materials is significant in both the normal and shear directions. With an increase in loading speed, the influence of the inertial effect on the deformation behaviour of materials increases gradually, and the initial yield stress of materials is significantly enhanced compared with that at low speed (v = 0.1 m/s).

4.4 Energy-absorption characteristics

The total energy absorption per unit volume of the honeycomb was used, and the expression is as follows.

$$E_A = \int_{\varepsilon_y}^{\varepsilon_d} \sigma(\varepsilon) d\varepsilon \tag{7}$$

where ε_d and ε_y are the densification and yield strains of the material, respectively.

Figures 29-31 show the total energy absorption of the auxetic honeycomb under different combined loading conditions. With an increase in the loading angle, the total energy absorption in the normal and shear directions of the material showed downward and upward trends, respectively. Owing to the increase in the loading angle, the shear deformation and stress of the honeycomb were significantly improved, and the extrusion between the cell wall and rib band was sufficient to significantly enhance the shear energy absorption of the material. However, for the overall energy absorption of the material, the total energy absorption in the normal direction was still significantly higher than that in the shear direction, thus occupying a dominant position.

When loading at low speeds, owing to the overall rotation and deformation of material cells, the normal energy absorption of materials at different loading angles is similar as a whole. Under medium- and high-speed loading conditions, the overall energy absorption of the material increases owing to the increased inertia effect. At this time, the loading angle significantly affects the energy absorption of the honeycomb in the normal and shear directions.

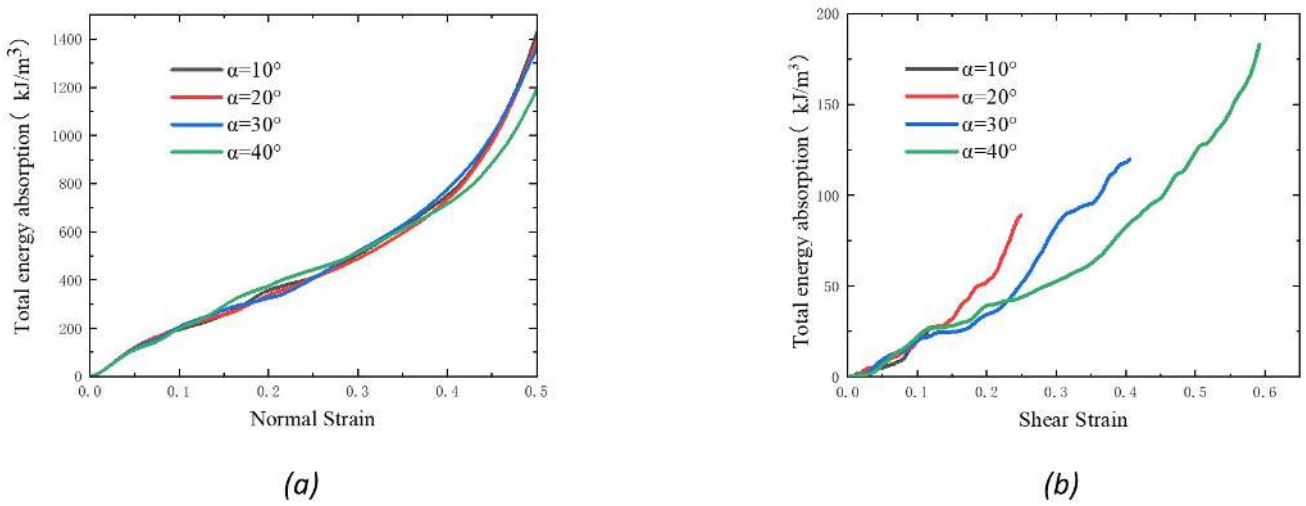

Figure 29. Total energy absorption of star-shaped auxetic honeycomb (v = 0.1 m/s): (a) Normal direction; (b) Shear direction.

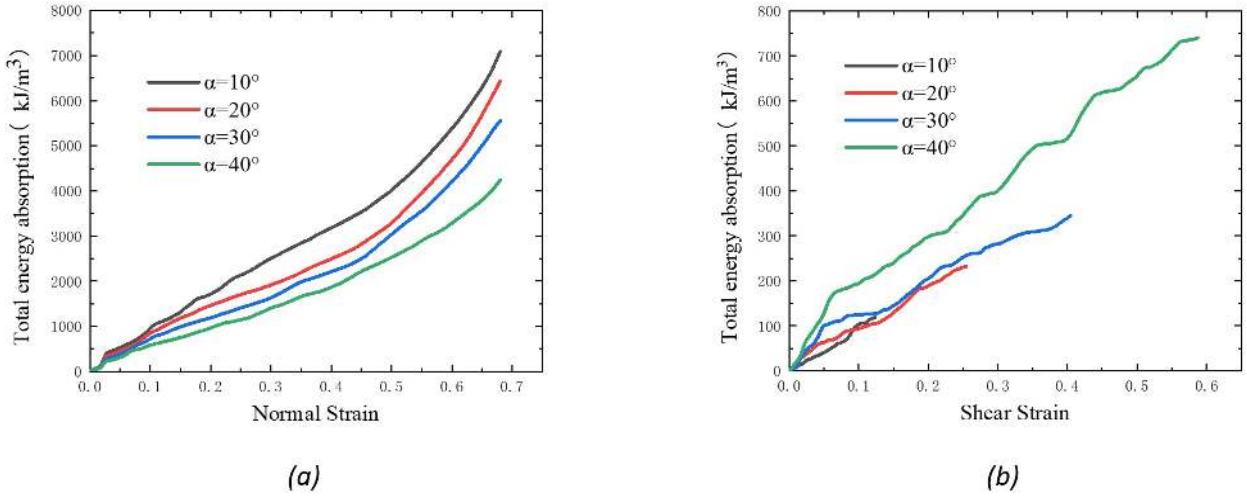

Figure 30. Total energy absorption of star-shaped auxetic honeycomb (v = 40 m/s): (a) Normal direction; (b) Shear direction.

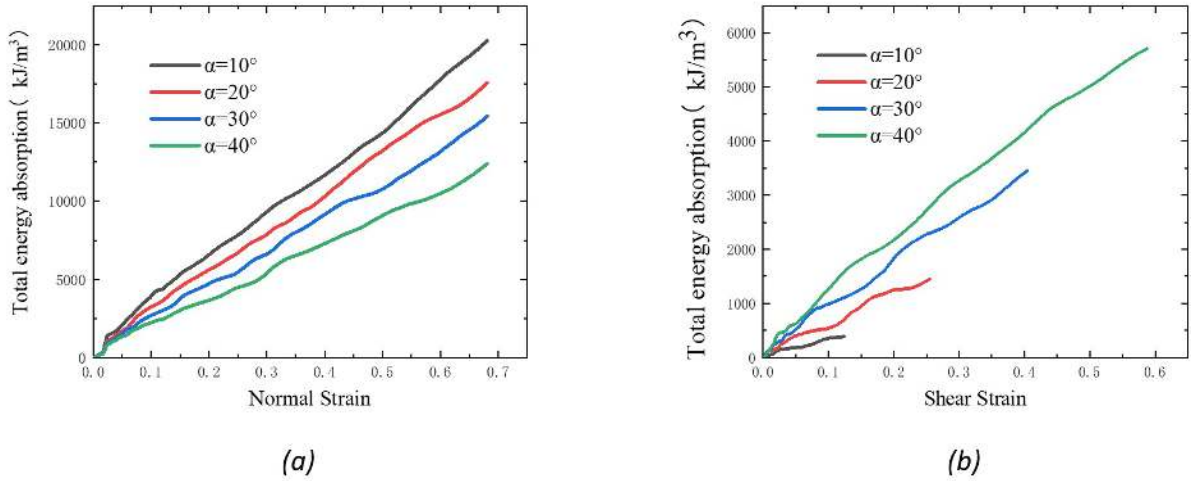

Figure 31. Total energy absorption of star-shaped auxetic honeycomb (v = 120 m/s): (a) Normal direction; (b) Shear direction.

As discussed in Section 4.1, the deformation mode of the honeycomb changes into crushing deformation dominated by plastic shock waves under high-speed loading. At this time, the impact energy was converted into two parts. One part of the energy was converted into deformation energy dissipated by the deformation and extrusion of the cell wall, which

is defined as the internal energy; and the rest was the kinetic energy of the plastic shock wave band moving with the loading plate. Under quasi-static compression, the honeycomb converts all the energy absorbed into internal energy through the deformation of the cell wall. The relationship is given by

$$E_d = E_N^d + E_S^d \tag{8}$$

$$E_{qs} = E_N^{qs} + E_S^{qs} \tag{9}$$

where E_d and E_{qs} are the total energy absorption of the honeycomb under dynamic and quasi-static loadings, respectively (kJ/m3); E_N^d and E_S^d are the total normal and shear energy absorptions of the honeycomb under dynamic loading, respectively (kJ/m^3); and E_N^{qs} and E_S^{qs} are the total normal and shear energy absorptions of the honeycomb under quasi-static loading, respectively (kJ/m^3).

The star-shaped auxetic honeycomb is anisotropic in-plane, and its normal and shear energy-absorption characteristics are independent of each other (Y. Mosleh et al, 2017). Therefore, the normal and shear energy-absorption characteristics of the material can be discussed separately. The normal energy-absorption relationship of the materials is as follows:

$$E_N^d = E_K^N + E_{Ni}^d = \sigma_d \varepsilon_N \tag{10}$$

$$E_N^{qs} = E_{Ni}^{qs} = \sigma_{qs} \varepsilon_N \tag{11}$$

where E_K^N and E_{Ni}^d are the normal components of the kinetic energy and normal internal energy of the honeycomb under dynamic loading, respectively (kJ/m^3); σ_d and σ_{qs} are the normal platform stresses of the honeycomb under dynamic and quasi-static loadings, respectively (MPa); and ε_N is the normal nominal strain of the honeycomb.
The shear energy absorption relationship of the materials is given by

$$E_S^d = E_K^S + E_{Si}^d = \tau_d \varepsilon_S \tag{12}$$

$$E_S^{qs} = E_{Si}^{qs} = \tau_{qs} \varepsilon_S \tag{13}$$

where E_K^S and E_{Si}^d are the shear components of the kinetic energy and shear internal energy of the honeycomb under dynamic loading, respectively (kJ/m^3); τ_d and τ_{qs} are the shear platform stresses under dynamic and quasi-static loadings of the honeycomb, respectively (MPa); ε_S is the nominal shear strain of the honeycomb.

By subtracting Equations (11) and (13) from Equations (10) and (12), respectively, the difference between the normal and shear dynamic internal energies and the quasi-static internal energy of the honeycomb can be obtained as follows:

$$\Delta E_i^N = E_{Ni}^d - E_{Ni}^{qs} = \sigma_d \varepsilon_N - \sigma_{qs} \varepsilon_N - E_K^N \tag{14}$$

$$\Delta E_i^S = E_{Si}^d - E_{Si}^{qs} = \tau_d \varepsilon_S - \tau_{qs} \varepsilon_S - E_K^S \tag{15}$$

where ΔE_i^N and ΔE_i^S represent normal and shear internal energy difference of honeycomb, respectively.

The dynamic and quasi-static platform stresses of materials satisfy the following relationship (G. Luo, and P. Xue, 2018):

$$\sigma_d = \sigma_{qs} + \frac{\rho_0 v_{Ni}^2}{\varepsilon_{Nd}} \tag{16}$$

$$\tau_d = \tau_{qs} + \frac{\rho_0 v_{Si}^2}{\varepsilon_{Sd}} \tag{17}$$

$$v_{Ni} = v_i \cos\alpha \tag{18}$$

$$v_{Si} = v_i \sin\alpha \tag{19}$$

where ρ_0 is the relative density of the honeycomb, v_i is the loading speed (m/s), v_{Ni} is the normal component of the loading speed (m/s), v_{Si} is the shear component of the loading speed (m/s), α is the combined compression-shear loading angle (°), and ε_{Nd} and ε_{Sd} are the normal and shear densification strains of the honeycomb, respectively.

By introducing Equations. (16) - (19) into Equations (14) and (15), we obtain the equations:

$$\Delta E_i^N = \frac{\rho_0 (v_i \cos\alpha)^2}{\varepsilon_{Nd}} \varepsilon_N - E_K^N \tag{20}$$

$$\Delta E_i^S = \frac{\rho_0 (v_i \sin\alpha)^2}{\varepsilon_{Sd}} \varepsilon_S - E_K^S \tag{21}$$

Under the high-speed loading condition, the cells behind the shock wave moved with the loading plate, while the cells in the wave front remained stationary with the support end. Thus, E_K^N and E_K^S can be expressed as

$$E_K^N = \frac{1}{2V_0} m_s v_{Ni}^2 = \frac{1}{2V_0} \left[V_0\rho_0 - S(L_0 - v_p t)\rho_0\right](v_i \cos\alpha)^2 \tag{22}$$

$$E_K^S = \frac{1}{2V_0} m_s v_{Si}^2 = \frac{1}{2V_0} \left[V_0\rho_0 - S(L_0 - v_p t)\rho_0\right](v_i \sin\alpha)^2 \tag{23}$$

where V_0 is the initial volume of the honeycomb (m^3), m_s is the mass of the cell after the wave (kg), S is the cross-sectional area of the honeycomb in the loading direction (m^2), v_p is the plastic shockwave velocity (m/s), and t is the loading time (s).

Under high-speed loading, the relationship between the plastic shock wave and the loading velocities is as follows (G. Luo, and P. Xue, 2018).

$$v_p = \frac{v_i}{\varepsilon_d} \tag{24}$$

It should be noted that the above relationship can only be satisfied when the direction of loading speed v_i and densification strain ε_d in Equation (24) is the same as that of the plastic shock wave. Under the combined loading condition, the normal component of the shock wave of the star-shaped honeycomb was consistent with the normal component of the loading speed (Figure 32). Therefore, under the combined loading condition,

$$v_p = \frac{v_{Ni}}{\varepsilon_{Nd}}. \tag{25}$$

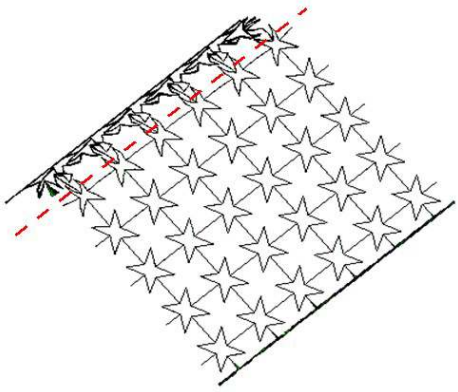

Figure 32. Plastic shock wave of star-shaped auxetic honeycomb.

By introducing Equation (24) into Equations (21) and (22), we obtain

$$E_K^N = \frac{\varepsilon_N}{2\varepsilon_{Nd}} \rho_0 (v_i \cos\alpha)^2 \tag{26}$$

$$E_K^S = \frac{\varepsilon_N}{2\varepsilon_{Nd}} \rho_0 (v_i \sin\alpha)^2 \tag{27}$$

By introducing Equation (26) and Equation (27) into Equation (20) and Equation (21), we obtain.

$$\Delta E_i^N = \frac{\varepsilon_N}{2\varepsilon_{Nd}}\rho_0(v_i\cos\alpha)^2 \tag{28}$$

$$\Delta E_i^S = \frac{(2tan\alpha-k)\varepsilon_N}{2k\varepsilon_{Nd}}\rho_0(v_i\cos\alpha)^2 \tag{29}$$

where $k = \frac{\varepsilon_{Sd}}{\varepsilon_{Nd}}$ is the ratio of the shear densification strain to the normal densification strain of honeycomb.

It can be observed from Equations (26) and (28) that the normal kinetic energy of a star-shaped auxetic honeycomb under high-speed loading is equal to its normal internal energy difference, which is related to the loading angle and impact speed. Simultaneously, the shear internal energy difference is related to the ratio k between the normal and shear densification strains. The comparisons between simulation results and theoretical values of kinetic energy of star-shaped auxetic honeycomb under different speeds are shown in Figures 33-35. It can be found that when the strain is less than 0.3, the theoretical model fits well with the simulation results. This is because the plastic shock wave of the material is no longer evident in the late stage of loading, and the theoretical model overestimates the kinetic energy of the honeycomb.

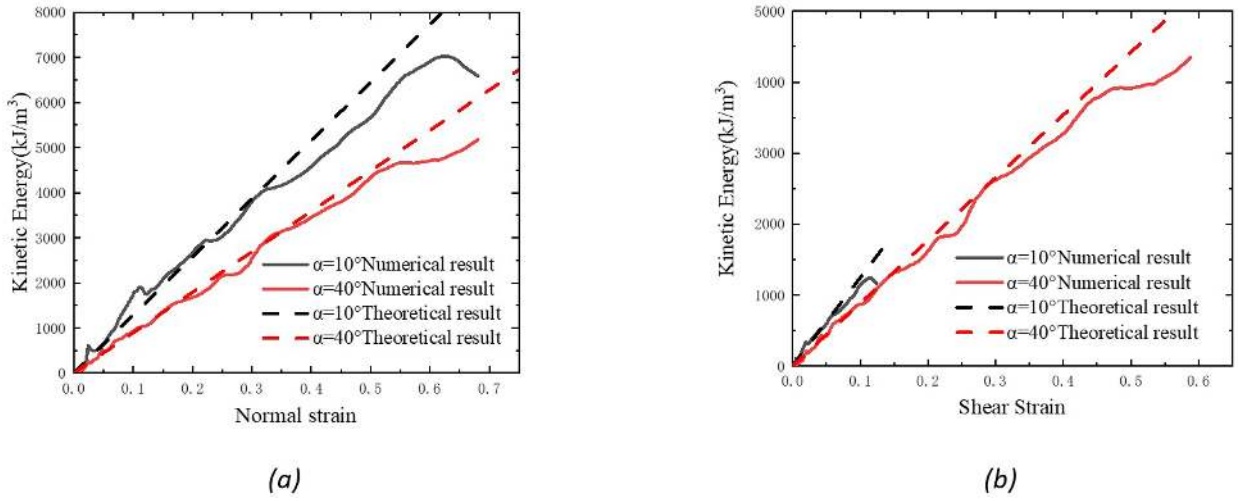

Figure 33. Comparison between simulation results and theoretical values of kinetic energy of star-shaped auxetic honeycomb under high-speed loading (v = 120 m/s): (a) Normal; (b) Shear

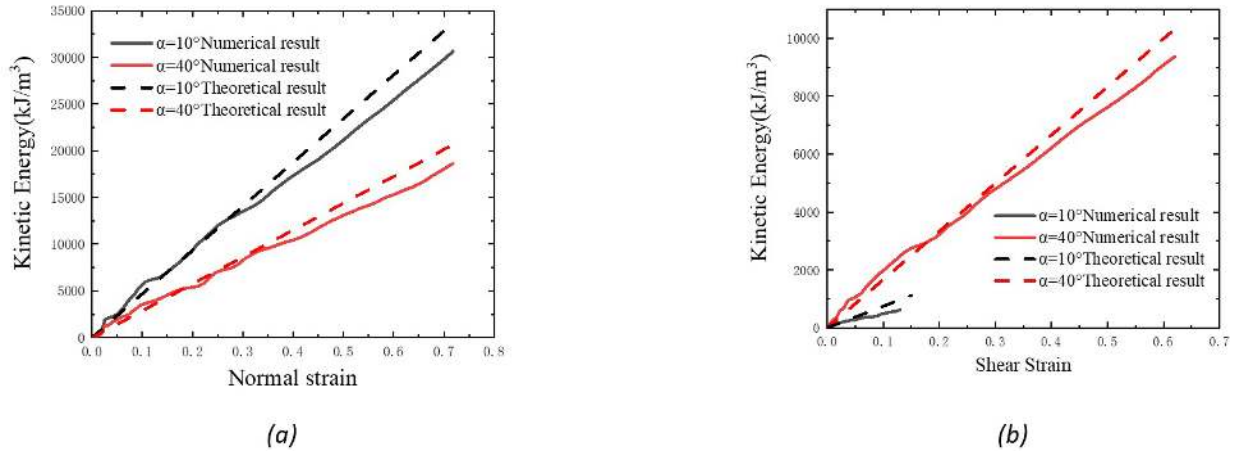

Figure 34. Comparison between simulation results and theoretical values of kinetic energy of star-shaped auxetic honeycomb under high-speed loading (v = 150 m/s): (a) Normal; (b) Shear

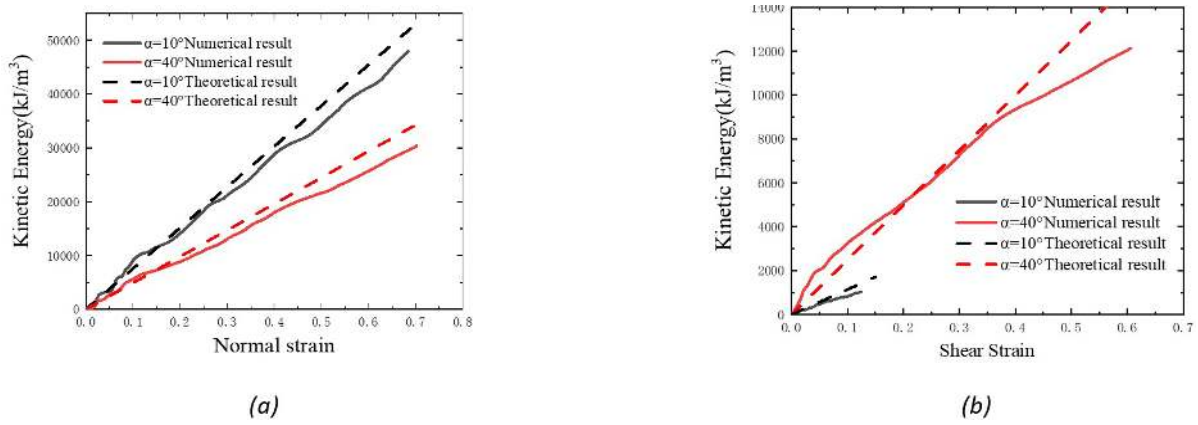

Figure 35. Comparison between simulation results and theoretical values of kinetic energy of star-shaped auxetic honeycomb under high-speed loading (v = 200 m/s): (a) Normal; (b) Shear

5. CONCLUSION

In this study, the mechanics and energy-absorption properties of star-shaped auxetic honeycombs were investigated. The specimens were prepared using additive manufacturing technology, and a quasi-static combined compression–shear experiment was conducted. Numerical models were established to achieve a dynamic combined loading, and theoretical models were derived to predict the yield behaviour and energy-absorption behaviour. The conclusions are as follows.

1. With an increase in loading speed, the deformation mode of the star-shaped auxetic honeycomb changes from overall deformation to progressive deformation and collapse deformation under combined loading.
2. The shear stress of the auxetic honeycomb under combined loadings is more sensitive to the loading angles. Hardening coefficients are defined to represent the influence of loading speed on the mechanical properties of the honeycomb, and the yield criterion of the material is given by ellipse fitting.
3. With an increase in the loading angle, the normal total energy absorption and shear total energy absorption of the material showed decreasing and increasing trends, respectively. Moreover, the normal kinetic energy of materials under dynamic loading is equal to the increase in internal energy compared with quasi-static loading, and the increase in internal energy in the shear direction is related to the ratio of densification strain in the shear and normal directions of the materials.

Acknowledgment

This work was supported by Natural Science Foundation of Shaanxi Province (2021JQ-220), and State Key Laboratory of Advanced Design and Manufacturing for Vehicle Body, Hunan University (32015006). We would like to thank Editage (www.editage.cn) for English language editing.

Author's Contribuitions: Conceptualization, Geng Luo and Duanyu Mo; Methodology, Yisong Chen; Investigation, Geng Luo, Duanyu Mo, Chengpeng Chai and Junzhe Liu; Writing - original draft, Duanyu Mo, Chengpeng Chai and Junzhe Liu; Writing - review & editing, Geng Luo and Yisong Chen.

Editor: Marcílio Alves

References

A. Ashab, D. Ruan, G. X. Lu et al., (2014) Combined Compression-Shear Behavior of Aluminum Honeycombs, Key Engineering Materials, 626:127-132.

A. Ingrole, A. Hao, and R. Liang, (2017) Design and modeling of auxetic and hybrid honeycomb structures for in-plane property enhancement, Materials & Design,117:72-83.

A. S. M. Ashab, D. Ruan, G. Lu et al., (2016) Quasi-static and dynamic experiments of aluminum honeycombs under combined compression-shear loading, Materials & Design, 97:183-194.

B. Hou, A. Ono, S. Abdennadher et al., (2011a) Impact behavior of honeycombs under combined shear-compression. Part I: Experiments, International Journal of Solids and Structures,48(5):687-697.

B. Hou, S. Pattofatto, Y. L. Li et al., (2011b) Impact behavior of honeycombs under combined shear-compression. Part II: Analysis, International Journal of Solids and Structures, 48(5):698-705.

C. Qi, F. Jiang, C. Yu et al., (2019), In-plane crushing response of tetra-chiral honeycombs, International Journal of Impact Engineering, 130:247-265.

C. Qi, F. Jiang, S. Yang et al., (2022) Dynamic crushing response of novel re-entrant circular auxetic honeycombs: Numerical simulation and theoretical analysis, Aerospace Science and Technology, 124.

C. Yang, and S. Kyriakides, (2019) Multiaxial crushing of open-cell foams, International Journal of Solids and Structures, 159:239-256.

F. Xu, K. Yu, and L. Hua, (2021) In-plane dynamic response and multi-objective optimization of negative Poisson's ratio (NPR) honeycomb structures with sinusoidal curve, Composite Structures,269.

G. Luo, and P. Xue, (2018) Investigations on the mechanism and behavior of dynamic energy absorption of metal foam,Latin American Journal of Solids and Structures,15(6).

Gibson, L. J., Ashby, M. F., Schajer, G., & Robertson, C. (1982). The mechanics of two-dimensional cellular materials. Proceedings of the Royal Society of London. A. Mathematical and Physical Sciences, 382(1782): 25-42.

H. Wang, Z. Lu, Z. Yang et al., (2019) In-plane dynamic crushing behaviors of a novel auxetic honeycomb with two plateau stress regions, International Journal of Mechanical Sciences, 151:746-759.

I. Gibson, and M. F. Ashby, (1982). The mechanics of three-dimensional cellular materials," Proceedings of the Royal Society of London. A. Mathematical and Physical Sciences, 382(1782):43-59.

J. Qiao, and C. Q. Chen, (2015) "Analyses on the In-Plane Impact Resistance of Auxetic Double Arrowhead Honeycombs," Journal of Applied Mechanics,82(5).

L. Li, P. Xue, and G. Luo, (2016) A numerical study on deformation mode and strength enhancement of metal foam under dynamic loading, Materials & Design, 110:72-79.

L. Wei, X. Zhao, Q. Yu et al., (2020) A novel star auxetic honeycomb with enhanced in-plane crushing strength, Thin-Walled Structures, 149.

L. Wei, X. Zhao, Q. Yu et al., (2021) Quasi-static axial compressive properties and energy absorption of star-triangular auxetic honeycomb, Composite Structures.

Lakes, R. (1987). Foam structures with a negative Poisson's ratio. Science, 235(4792):1038-1040.

M. Doyoyo, and D. Mohr, (2003) Microstructural response of aluminum honeycomb to combined out-of-plane loading, Mechanics of Materials,35(9):865-876.

M. Xu, D. Liu, P. Wang et al., (2020). In-plane compression behavior of hybrid honeycomb metastructures: Theoretical and experimental studies, Aerospace Science and Technology, 106.

Obadimu, Solomon O.; Kourousis, Kyriakos I, (2023) In-plane compression performance of additively manufactured honeycomb structures: a review of influencing factors and optimisation techniques. International Journal of Structural Integrity.

R. A. W. Mines, S. Tsopanos, Y. Shen et al., (2013), Drop weight impact behaviour of sandwich panels with metallic micro lattice cores, International Journal of Impact Engineering,60:120-132.

R. Gümrük, and R. A. W. Mines, (2013) Compressive behaviour of stainless steel micro-lattice structures, International Journal of Mechanical Sciences, 68:125-139.

S. D. Rapaka, M. Pandey, and R. K. Annabattula, (2020). Dynamic compressive behavior of auxetic and non-auxetic hexagonal honeycombs with entrapped gas. International Journal of Impact Engineering, 146.

S. Hong, J. Pan, T. Tyan et al., (2008) Dynamic crush behaviors of aluminum honeycomb specimens under compression dominant inclined loads, International Journal of Plasticity,24(1): 89-117.

T. Wang, Z. Li, L. Wang et al., (2022). In-plane elasticity of a novel arcwall-based double-arrowed auxetic honeycomb design: Energy-based theoretical analysis and simulation," Aerospace Science and Technology, 127.

X. Niu, F. Xu, Z. Zou et al., (2022), In-plane dynamic crashing behavior and energy absorption of novel bionic honeycomb structures, Composite Structures, 299.

Y. Mosleh, K. Vanden Bosche, B. Depreitere et al., (2017) Effect of polymer foam anisotropy on energy absorption during combined shear-compression loading, Journal of Cellular Plastics,54(3): 597-613.

Z. Dong, Y. Li, T. Zhao et al., (2019) Experimental and numerical studies on the compressive mechanical properties of the metallic auxetic reentrant honeycomb, Materials & Design, 182.